AGU PUBLICATIONS

Geophysical Research Letters

RESEARCH LETTER
10.1002/2015GL065529

Key Points:
- A single parameter controls the evaporative amplification of entrainment
- Only part of the evaporative cooling contributes to the entrainment velocity
- The analysis reconciles many previous entrainment velocity parameterizations

Correspondence to:
A. de Lozar,
adelozar@gmail.com

Citation:
de Lozar, A., and J. P. Mellado (2015), Evaporative cooling amplification of the entrainment velocity in radiatively driven stratocumulus, *Geophys. Res. Lett.*, *42*, 7223–7229, doi:10.1002/2015GL065529.

Received 27 JUL 2015
Accepted 17 AUG 2015
Accepted article online 20 AUG 2015
Published online 15 SEP 2015

Evaporative cooling amplification of the entrainment velocity in radiatively driven stratocumulus

Alberto de Lozar[1] and Juan Pedro Mellado[1]

[1] Max Planck Institute for Meteorology, Hamburg, Germany

Abstract Evaporative cooling monotonically increases as the thermodynamical properties of the inversion allow for more evaporation in shear-free radiatively driven stratocumulus. However, the entrainment velocity can deviate from the evaporative cooling trend and even become insensitive to variations in the inversion properties. Here the efficiency of evaporative cooling at amplifying the entrainment velocity is quantified by means of direct numerical simulations of a cloud top mixing layer. We demonstrate that variations in the efficiency modulate the effect of evaporative cooling on entrainment, explaining the different trends. These variations are associated with the evaporation of droplets in cloud holes below the inversion point. The parametrization of the efficiency provides the evaporative amplification of the entrainment velocity as a function of a single parameter that characterizes the inversion. The resulting entrainment velocities match our experiments and previous measurements to within ±25%. The parametrization also predicts the transition to a broken-cloud field consistently with observations.

1. Introduction

Stratocumuli are shallow, stratiform clouds that spread over several hundreds of kilometers in the subtropical regions. They cover around 20% of the Earth and are thus key for the Earth's radiation balance. Current knowledge of the stratocumulus mixing dynamics is, however, insufficient, causing uncertainty in weather prediction and climate models [*Wood*, 2012].

The main drivers of the stratocumulus dynamics are often long-wave radiative and evaporative cooling. At the top of the cloud, long-wave radiation cools cloud parcels that become negatively buoyant and generate turbulence as they fall through the cloud. Turbulence promotes the entrainment of dry and warm air parcels from the free atmosphere. The entrained parcels are positively buoyant, but this can be compensated by the cooling associated with the evaporation of cloud droplets. The buoyancy reversal instability (BRI) happens when the evaporative cooling overcomes the positive buoyancy of the entrained parcels. The BRI closes a positive feedback between turbulence and entrainment that might lead to cloud breakup, a scenario known as the cloud top entrainment instability (CTEI) [*Randall*, 1980; *Deardorff*, 1980]. However, the relative importance of the CTEI and of the BRI for the boundary layer dynamics remain unknown [*Wood*, 2012].

Current parameterizations of the entrainment velocity, which quantifies the mixing of the cloud with the free atmosphere, differ by a factor of order 1 [*Stevens*, 2002]. These differences can be partly explained by comparing the relative importance of evaporative and radiative cooling in each parameterization. In one limit, *Turton and Nicholls* [1987] consider that the entrainment velocity is mainly determined by the interaction of turbulence with evaporative cooling, and they include the radiative forcing only as a generic source of turbulence. In the other limit, *Moeng* [2000] and *Lock* [1998] implicitly assume that the entrainment velocity is determined only by radiative cooling and turbulence. Between these limits, the parameterizations of *Lilly* [2002] and *Lock and MacVean* [1999] consider both evaporative and radiative cooling, although they introduce these forcings quite differently. In summary, present parameterizations disagree even on which mechanisms are relevant for the entrainment.

In this paper we investigate the amplification of the entrainment velocity by evaporative cooling in a cloud top mixing layer driven by radiative and evaporative cooling in the limit of negligible mean shear. The analysis is based on the formulation and direct numerical simulations (DNS) presented in *de Lozar and Mellado* [2015] (henceforth LM2015). The main strength of this study is that DNS combined with the new formulation allows us to directly quantify the evaporative and radiative cooling contributions to the entrainment velocity.

2. Analysis

We consider a cloud top mixing layer that mimics the stratocumulus top. This system consists of a moist layer, the cloud, that lies below a dryer and warmer layer, which represents the free atmosphere. We focus on cases in which the buoyancy difference between both layers, Δb, is strong enough to keep a relatively flat interface: $(\Delta b)T_c\, g^{-1} \sim 3\text{–}10$K, where T_c is the cloud layer temperature. The long-wave radiation is characterized by the reference buoyancy flux $B_0 = F_0 g(\rho c_p T_c)^{-1}$, where F_0 is the radiation flux, and by the radiative extinction length, $\lambda \sim 15$ m, that defines the region cooled by radiation [*Larson et al.*, 2007]. The evaporative cooling is characterized by the saturation mixing ratio, χ_s, and by the normalized buoyancy of the just saturated cloud-dry-air mixture $D = -b(\chi_s)/\Delta b$ [*Siems et al.*, 1990].

In this paper we use the parameter $(D/\chi_s + 1)$ as a measure for the potential of the inversion for evaporative cooling. The first reason for this choice is that this parameter quantifies the relative differences in buoyancy caused by the evaporative cooling:

$$(D/\chi_s + 1) = \left[b_{\mathrm{lm}}(\chi_s) - b(\chi_s)\right]/b_{\mathrm{lm}}(\chi_s), \tag{1}$$

where b_{lm} is the linearly mixing buoyancy function, which is obtained when neglecting evaporative cooling. The second reason is that $(D/\chi_s + 1)$ directly relates the integrated variation of buoyancy due to evaporative cooling to the entrainment velocity in a quasi-steady state (shown below by equation (4)). The limit $(D/\chi_s + 1) \to 0$ corresponds to a negligible effect of the evaporative cooling. As this parameter grows, we expect an increase of the effect of the evaporative cooling on the buoyancy and consequently also on the entrainment velocity. The condition $D > 0$ or $(D/\chi_s + 1) > 1$ corresponds to the onset of the BRI.

2.1. The Integrated Buoyancy Equation

We choose the inversion point as the point of neutral buoyancy ($\langle b\rangle(z_i) = 0$, where $\langle\rangle$ means horizontal averages). We identify the entrainment zone as the region above the inversion point and the in-cloud zone as the region below it. This partition is thoroughly justified in LM2015. The integration of the buoyancy evolution equation in the entrainment zone leads to the next decomposition:

$$-\frac{\mathrm{d}}{\mathrm{d}t}\int_{z_i}^{\infty}\langle b\rangle \mathrm{d}z = \left(w_e + w_e^{\mathrm{diff}}\right)\Delta b = \underbrace{-\langle w'b'\rangle_{z_i} + \kappa_t\left\langle\frac{\partial b}{\partial z}\right\rangle_{z_i} + \int_{z_i}^{\infty}\langle s_{\mathrm{rad}}\rangle \mathrm{d}z}_{w_e^{\mathrm{rad}}\Delta b} + \underbrace{\int_{z_i}^{\infty}\langle s_{\mathrm{eva}}\rangle \mathrm{d}z}_{\left(w_e^{\mathrm{eva}}+w_e^{\mathrm{diff}}\right)\Delta b}, \tag{2}$$

where s_{rad} and s_{eva} are the buoyancy source terms due to radiative and evaporative cooling, respectively, as defined in LM2015. Equation (2) defines the next entrainment velocities:

- w_e quantifies the temporal variations of the integrated buoyancy above the cloud, once the diffusive contribution w_e^{diff} discussed below is removed. In the quasi-steady state w_e quantifies the mixing of a conserved scalar between the free atmosphere and the cloud [see *de Lozar and Mellado*, 2013]. This form of the entrainment velocity reduces to $w_e = \mathrm{d}z_i/\mathrm{d}t$, if the diffusive and deformation terms can be neglected (LM2015). The inviscid scalings presented in LM2015 strongly suggest that w_e is sufficiently resolved in our simulations to extrapolate to atmospheric conditions.
- w_e^{diff} quantifies the diffusive entrainment by evaporative cooling alone, due to the BRI. The instability that leads to this diffusive entrainment was investigated and quantified in *Mellado* [2010], in a configuration solely driven by evaporative cooling. In LM2015 we show that the same analysis can be applied for cases with radiative cooling and a strong stratification. w_e^{diff} is very small for air viscosity, but it can reach values comparable to the total entrainment rate for viscosities typically employed in stratocumulus simulations.
- w_e^{rad} quantifies the entrainment velocity due to the combined action of radiative cooling and the buoyancy flux at the inversion point. In LM2015 we show that w_e^{rad} is independent of the evaporative cooling process. For cases with strong stratification this entrainment velocity is well approximated by

$$w_e^{\mathrm{rad}}\Delta b = \left[0.175 + 0.78(w^*)^2/(\lambda\Delta b)\right]\beta B_0, \tag{3}$$

where w^* is the integral velocity calculated from the integrated buoyancy flux and $\beta \simeq 0.5$ relates the changes in buoyancy to the variations in enthalpy (similar as in *Randall* [1980]). When $\beta = 1$, equation (3) is equivalent

to the parameterization for the entrainment velocity in a smoke cloud with no evaporative cooling [*de Lozar and Mellado*, 2013]. These parameterizations were developed for cases without a surface buoyancy flux or mean shear, which should be accounted for in a more general framework.

- w_e^{eva} quantifies the contribution to the entrainment velocity due to the evaporative cooling at the entrainment zone, once the diffusive contribution is removed. The investigation of this contribution is the subject of the next subsection.

2.2. The Evaporative Cooling Contribution

Our starting point is the balance between the total evaporative cooling buoyancy source, S_{eva}, and the entrainment velocity:

$$S_{eva} = \int_0^\infty \langle s_{eva} \rangle dz = \left(w_e + w_e^{diff} \right) \Delta b \left(D/\chi_s + 1 \right), \tag{4}$$

which is approached when the flow tends to a quasi-steady state (LM2015).

The next step is to relate the total evaporative cooling, S_{eva}, to the evaporative cooling contribution to the entrainment velocity, w_e^{eva}. While the limits of the integral that defines S_{eva} in equation (4) include both the in-cloud and entrainment zone, the limits of the integral that defines $w_e^{eva}\Delta b$ in equation (2) only account for the entrainment zone (defined by $z > z_i$). This means that the total evaporative cooling is equal to the evaporative cooling contribution to the entrainment velocity only if all evaporation occurs in the entrainment zone. Throughout this paper, we show that the condition $S_{eva} = w_e^{eva}\Delta b$ only applies for cases with weak evaporative cooling ($(D/\chi_s + 1) \sim 0$). In cases with stronger evaporative cooling, part of the evaporation happens far from the entrainment zone and does not contribute directly to the entrainment process.

Based on the previous considerations, we define the efficiency, ϵ, as the fraction of the evaporative cooling that happens at the entrainment zone, thus having a direct impact on the entrainment velocity:

$$\epsilon = \frac{\int_{z_i}^\infty \langle s_{eva} \rangle dz - w_e^{diff}\Delta b}{\int_0^\infty \langle s_{eva} \rangle dz - w_e^{diff}\Delta b (D/\chi_s + 1)} = \frac{w_e^{eva}\Delta b}{S_{eva} - w_e^{diff}\Delta b (D/\chi_s + 1)}, \tag{5}$$

where we have removed the diffusive contributions from the BRI. The efficiency is equivalent to the fraction of direct cooling for the long-wave radiative forcing, as originally introduced by [*Lilly*, 1968]. In the limit $\epsilon = 0$ the evaporative cooling has no direct effect on the entrainment. In the limit $\epsilon = 1$ all evaporative cooling from the inviscid contribution enhances the entrainment velocity. The efficiency plays a similar role in the integrated buoyancy equation as the wetness introduced by *Lilly* [2002] and behaves identically in both limiting cases. We prefer to use the efficiency because it can be directly quantified in our simulations by using equation (5), while the wetness has to be a posteriori inferred from the entrainment velocity.

In order to provide a physical picture for the efficiency, we consider an entrainment scenario similar to the one described in *Gerber et al.* [2005], *Kurowski et al.* [2009], and *Yamaguchi and Randall* [2012]. According to this scenario, recently entrained parcels are positively buoyant and stay in the entrainment zone (roughly equal to the entrainment interfacial layer in those references). In a first stage, mixing, evaporation, and long-wave radiation cool those parcels, until their buoyancy is similar to the cloud buoyancy. In a second stage, the entrained parcels, which are now approximately neutrally buoyant, are swept from the entrainment zone into the inner part of the cloud by the convective movements. These parcels converge into the holes that characterize the stratocumulus top [*Gerber et al.*, 2005]. Mixing continues during the second stage, and therefore the evaporation of droplets can also continue for parcels that still retain some unsaturated air. Within this conceptual framework we differentiate between the evaporative cooling during the first stage, which directly helps the entrainment by reducing the parcel buoyancy, and the evaporative cooling in the second stage, which does not help directly to the entrainment process because the parcels are already entrained. The efficiency can be understood as the fraction of the total evaporative cooling that happens during the first stage of the entrainment process, which is more efficient in generating entrainment.

Combining equations (2), (4), and (5) yields

$$w_e = A_{eva} w_e^{rad} = \frac{w_e^{rad}}{1 - \epsilon \left(D/\chi_s + 1 \right)}, \tag{6}$$

which shows that the evaporative cooling multiplies the effect of radiative cooling on the entrainment by an amplification factor A_{eva}. In the case of full efficiency ($\epsilon \equiv 1$), A_{eva} monotonically grows with $(D/\chi_s + 1)$ and

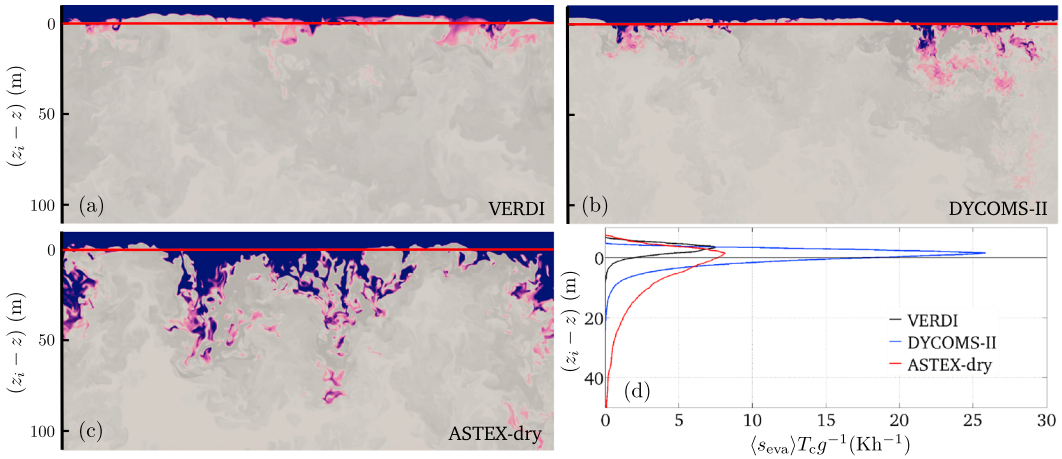

Figure 1. (a–c) Liquid water cross sections in experiments based on the field campaign indicated in the label. Details of each experiment can be found in the text. For all cases the integral length scale is $z^* \sim 100$ m and the simulation time is ~10 min, when assuming $\lambda = 15$ m. The red line indicates the height of the inversion point that separates the entrainment zone and the in-cloud region. (d) Horizontally averaged evaporative cooling buoyancy source. According to our analysis, only the evaporation that happens above the inversion point contributes directly to the entrainment velocity.

diverges for the BRI condition $D = 0$. Equation (6) thus recovers the Randall-Deardorf criterion for the CTEI in the limit $\epsilon \equiv 1$. Negative values of $A_{\rm eva}$ are identified with the runaway feedback between evaporative cooling and entrainment described by *Randall* [1980] and *Deardorff* [1980].

3. Results

In this section we investigate the dependency of the efficiency on $(D/\chi_s + 1)$ and show how a changing efficiency modulates the dependence of the entrainment velocity on the evaporative cooling parameters.

3.1. Visualizations

In order to show how the efficiency behaves in different regimes, we first investigate three cases that differ in the intensity of the evaporative cooling.

The first case is based on the measurements of the reference flight 11 from the VERtical Distribution of Ice in Arctic clouds (VERDI) campaign in the north of Canada [*Klingebiel et al.*, 2015]. This case is characterized by weak evaporative cooling, due to the small jump in humidity across the inversion ($\Delta q_{\rm t} = -0.65$ gkg^{-1}, $D/\chi_s + 1 = 0.45$). Accordingly, this case is stable against the BRI. Figure 1a from our simulations shows that the mixing is mostly concentrated close to the cloud top and that only some small holes are able to penetrate a few meters. Many of these holes contain fully saturated air (in purple in Figure 1a), suggesting that most of the evaporation happens in the entrainment zone. This observation is confirmed by the horizontally averaged evaporative cooling buoyancy source profile in Figure 1d. Since most of the evaporation occurs in the entrainment zone, the efficiency for this case is very high ($\epsilon = 0.9$).

The second case is based on the measurements of the reference flight RF-01 from the Second Dynamics and Chemistry of Marine Stratocumulus field study (DYCOMS-II) campaign, close to the coast of California [*Stevens et al.*, 2005]. This case is characterized by a strong evaporative cooling due to a large jump in humidity ($\Delta q_{\rm t} = -7.5$ gkg^{-1}, $D/\chi_s + 1 = 1.34$). The inversion is unstable against the BRI, although observations did not show any cloud breaking. Figure 1b from our simulations shows a solid cloud deck with stronger mixing than in the previous case, pointing to a higher entrainment velocity. The cloud holes in DYCOMS-II penetrate deeper than in VERDI and have a drier composition. This is in agreement with *Gerber et al.* [2005], who frequently observed cloud holes that penetrate up to hundreds of meters during the DYCOMS-II campaign. Unsaturated dry air is evacuated from the entrainment zone through the holes into the cloud core, resulting in the evaporation of liquid in the in-cloud region (see Figure 1d). As a consequence, the efficiency notably departs from 1 ($\epsilon = 0.54$). This low efficiency partly compensates the intensification of the entrainment by a very dry free atmosphere and inhibits the CTEI.

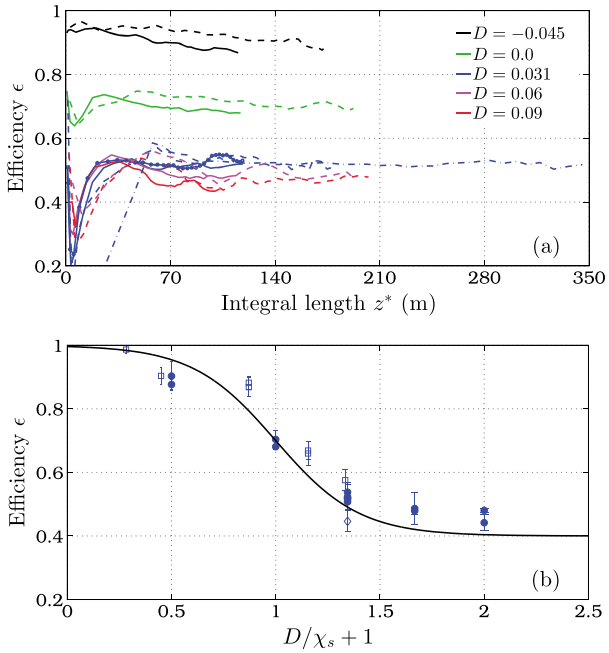

Figure 2. (a) Efficiency as a function of the integral length scale of the in-cloud turbulence. The reference case (in blue) corresponds to the DYCOMS-II simulation described in Figure 1. The other cases differ from the reference case in the evaporative cooling parameter D (coded by the color in the legend) and in the viscosity (coded by the line type). The viscosity is given in terms of $Re_0 = B_0^{1/3}\lambda^{4/3}\nu^{-1}$: circles for 1600, solid for 800, dashed for 400, and dash-dotted for 200. (b) Averaged efficiency from $z^* = 50$ m as a function of $(D/\chi_s + 1)$. The error bars represent the temporal variations, quantified by three standard deviations. Solid circles represent the cases shown in Figure 2a, for which $\chi_s = 0.09$. Open squares correspond to cases with $\chi_s > 0.09$ and the open diamond to $\chi_s = 0.045$. The line is given by equation (7).

The third case is motivated by the measurements of the reference flight A210 from the Atlantic Stratocumulus Transition Experiment (ASTEX) campaign in the Atlantic [*de Roode and Duynkerke*, 1997]. In order to create a case in which the evaporative cooling has a very strong effect ($D/\chi_s + 1$=2.45), we reduce the free atmosphere vapor content so that the jump in humidity is $\Delta q_t = -7.4$ gkg^{-1}, instead of the measured $\Delta q_t = -4.5$ gkg^{-1}. All other parameters in the simulation correspond to the measured properties. This case is unstable against the BRI, and the observations showed a broken stratocumulus deck. Figure 1c from our simulations shows dry-air holes that rapidly grow in size, at a rate comparable with the integral velocity of the in-cloud turbulence. We identify these unsteady dynamics with the breaking of the stratocumulus deck in observations. Due to such large holes, most of the evaporation occurs far from the entrainment zone and the efficiency is low ($\epsilon = 0.29$).

3.2. The Efficiency

Figure 2a shows the efficiency as a function of the integral length scale, z^*, which is approximately half of the boundary layer depth and thus characterizes the largest flow scale in the simulation (LM2015). In all cases the efficiency levels at a constant value after a short transient ($z^* < 50$ m), suggesting that ϵ will not vary appreciably for atmospheric scales ($z^* \sim 400-1000$ m). The efficiency is also independent of viscosity, which suggests that ϵ does not change either by viscous effects or by further resolving the small-scale turbulence. We conclude that the length scales relevant for the efficiency are well resolved in our simulations. This condition allows us to extrapolate our results to cloud scales.

In Figure 2a the efficiency decreases with increasing the parameter D, which quantifies the minimum buoyancy of an entrained parcel when it mixes with the cloud. Negative D corresponds to positively buoyant parcels that tend to stick to the entrainment zone, consistent with a high efficiency. Positive D corresponds to heavy parcels that can quickly escape the entrainment zone, lowering the efficiency.

When comparing cases with different χ_s, we observe a clear tendency of ϵ to increase with χ_s (not shown). This behavior can be explained by looking at an entrained dry-air parcel of volume dv_d. From the definition of χ_s, the volume of cloudy air dv_c necessary to bring the entrained parcel to saturation is $dv_c = dv_d(1-\chi_s)\chi_s^{-1}$. The time that it takes to saturate the entrained parcel thus increases with decreasing χ_s, because it involves mixing a larger amount of cloudy air dv_c. For low χ_s, dry-air parcels have time to penetrate deep into the cloud before saturation, resulting in a low efficiency. When χ_s is high the process of bringing the dry-air parcel to saturation is fast, resulting in a relatively large evaporation in the entrainment zone and a high efficiency.

From the previous considerations it becomes clear that the efficiency must be a function of the evaporative cooling parameters D and χ_s. Motivated by the physical meaning of $(D/\chi_s + 1)$ explained in section 2, we assume that the efficiency is a function of $(D/\chi_s + 1)$ only. Figure 2b shows that this simple assumption is valid up to small variations of around 0.05 that arise when varying χ_s in the interval $0.045 \leq \chi_s \leq 0.24$.

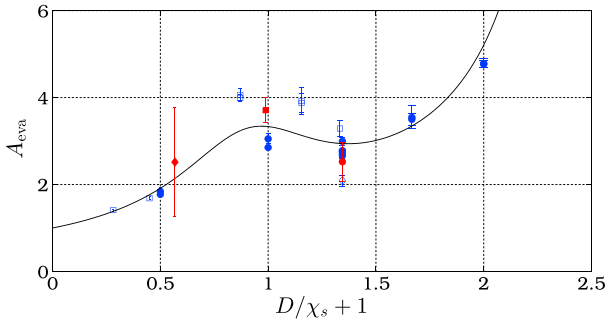

Figure 3. Amplification of the radiative entrainment velocity due to evaporative cooling (see equation (6)) as a function of the potential for evaporative cooling defined by $(D/\chi_s + 1)$. Blue markers are calculated from our simulations (legend in Figure 2). Red markers are calculated from measurements in nocturnal stratocumulus. The circle and the square correspond to the reference flights RF-01 [*Stevens et al.*, 2005] and RF-02 [*Ackerman et al.*, 2009] from the DYCOMS-II campaign. The diamond corresponds to the reference flight A209 from the ASTEX campaign [*de Roode and Duynkerke*, 1997]. The radiative entrainment velocity w_e^{rad} in the measurements is calculated by using equation (3) with an extinction length $\lambda = 15$ m. The line represents the parameterization given by equations (6) and (7).

The efficiency in Figure 2b shows two clear limiting values. In the limit of negligible evaporative cooling $((D/\chi_s+1) \to 0)$, the efficiency tends to 100% ($\epsilon_t = 1$). In the limit of a strong evaporative cooling $((D/\chi_s + 1) \gtrsim 1.5)$, the efficiency asymptotes to a constant value $\epsilon_l = 0.4$, which is the lowest possible efficiency in a quasi-steady state. Efficiencies below this limit ($\epsilon < 0.4$) are found only in simulations that display an unsteady, broken-cloud structure, like in Figure 1c. For this reason these low values are not included in Figure 2b.

3.3. The Entrainment Velocity Parameterization

In order to construct a parameterization for the entrainment velocity, we approximate the efficiency by the next function:

$$\epsilon = 0.7 - 0.3 \tanh\left[2.5(D/\chi_s)\right], \qquad (7)$$

which is represented in Figure 2b. Equation (7) meets both limits of the efficiency described above and connects them in a smooth way that approximates our measurements.

The assumption of writing the efficiency as a function of $(D/\chi_s + 1)$ allows us to write the evaporative cooling entrainment amplification A_{eva} as a function of $(D/\chi_s + 1)$ only, by combining equations (6) and (7). In Figure 3 we compare the resulting A_{eva} to the values from our simulations. The differences between the predicted A_{eva} and our measurements are ~20%, consistent with the validity of the assumptions we made during the analysis and with the statistical significance of the properties measured in our simulations. We include in Figure 3 three values of A_{eva}, which are derived from nocturnal flights measurements during the ASTEX [*de Roode and Duynkerke*, 1997] and DYCOMS-II [*Stevens et al.*, 2005; *Ackerman et al.*, 2009] campaigns. The evaporative cooling amplification derived from these observations deviates from our prediction by ~25%, similar to the simulations.

4. Discussion and Conclusions

We have demonstrated that the enhancement of the entrainment velocity by evaporative cooling does not increase monotonically as the inversion allows for more evaporation (see Figure 3). Instead, we identify three different regimes. The regimes differ on how sensitive the entrainment velocity is to variations of the potential of the inversion for evaporative cooling measured by $(D/\chi_s + 1)$.

For $(D/\chi_s+1) \gtrsim 0$, the entrainment velocity steadily increases with (D/χ_s+1) above the values corresponding to the radiative-only configurations. This regime is characterized by a very high efficiency ($\epsilon \simeq 1$ in Figure 2b). This means that most evaporation occurs in the entrainment zone (see Figure 1a) and serves to enhance the entrainment velocity. As a result, variations in the evaporative cooling properties of the inversion have a direct impact on the entrainment velocity. This behavior qualitatively agrees with the parameterization of *Turton and Nicholls* [1987].

For $(D/\chi_s + 1) \sim 1$ (close to the onset of the BRI) the entrainment velocity levels at $w_e \sim 3w_e^{rad}$ and becomes roughly independent of the evaporative cooling parameters. This regime is characterized by a strong decrease of the efficiency when increasing (D/χ_s+1), as shown in Figure 2b. The reduction in the efficiency is associated with the creation of cloud holes, in which part of the entrained dry air is transported deep into the cloud (see Figure 1b). This mechanism limits the capacity of evaporative cooling to strengthen the entrainment, because part of the evaporation now happens far from the entrainment zone, deep inside the cloud. This compensates the otherwise expected increase in the entrainment velocity by increasing the potential for evaporative cooling (higher $(D/\chi_s + 1)$). A constant entrainment velocity is consistent with the parameterizations of *Moeng* [2000] and *Lock* [1998], which are independent of the evaporative cooling parameters.

For $(D/\chi_s + 1) \gtrsim 1.5$ the entrainment velocity grows rapidly with $(D/\chi_s + 1)$. The efficiency in this regime approaches a limiting value $\epsilon_l \to 0.4$, which indicates that the above explained mechanisms for evacuating subsaturated air from the entrainment zone in a quasi-steady state cannot grow beyond a certain threshold. Equation (6) predicts that the entrainment velocity diverges for $(D/\chi_s + 1) = 2.5$. Our simulations show that the stratocumulus deck breaks in this limit, in the sense that the hole sizes grow at a rate comparable with the integral velocity of the in-cloud turbulence (see Figure 1c).

We identify the cloud breakup in our simulations with the CTEI. The condition for the CTEI is usually given in terms of $\kappa = \Delta\Theta_e/(L\Delta q_t)$ reaching a critical value κ_c at which the stratocumulus deck breaks. According to *Deardorff* [1980] and *Randall* [1980], the CTEI is initiated by the BRI condition, which they found at $\kappa_c = 0.23$. Our analysis suggests that this result comes from the implicit assumption that all evaporative cooling contributes to the entrainment (equation (6) diverges for the BRI condition when $\epsilon \equiv 1$). For the limiting efficiency suggested from our simulations $\epsilon_l = 0.4$, the divergent condition corresponds to $0.5 \leq \kappa_c \leq 0.75$ when using typical stratocumulus conditions ($\beta = 0.5$ and $0 \leq \chi_s \leq 0.4$). This condition is more in agreement with the analysis of the observations of *Kuo and Schubert* [1988] and with the CTEI criterion of *MacVean and Mason* [1990] ($\kappa_c \simeq 0.7$). The approximate agreement of this criterion with our CTEI condition is explained because both analyses introduce mechanisms that weaken the amplification of entrainment by evaporative cooling. An efficiency below 1 thus stabilizes the inversion against the BRI and shifts the CTEI to more unstable inversions.

In summary, the introduction of the concept of efficiency in the analysis of the entrainment velocity helps to describe different dynamics in stratocumulus driven by radiative and evaporative cooling. The resulting parameterization of the entrainment velocity reconciles many existing parameterizations, at least in a qualitative way. Further analysis should investigate how surface fluxes, short-wave radiation, and shear might alter this analysis.

Acknowledgments
All data used for this study will be provided upon request to anyone interested. Support from the Max Planck Society through its Max Planck Research Groups program is gratefully acknowledged. The authors are grateful to Stephan de Roode for providing the data from the ASTEX campaign. Computational time was provided by the Jülich Supercomputing Centre.

The Editor thanks two anonymous reviewers for their assistance in evaluating this paper.

References

Ackerman, A. S., et al. (2009), Large-eddy simulations of a drizzling, stratocumulus-topped marine boundary layer, *Mon. Weather Rev.*, *3*, 1083–1110.
de Lozar, A., and J. P. Mellado (2013), Direct numerical simulations of a smoke cloud-top mixing layer as a model for stratocumuli, *J. Atmos. Sci.*, *70*(8), 2356–2375, doi:10.1175/JAS-D-12-0333.1.
de Lozar, A., and J. P. Mellado (2015), Mixing driven by radiative and evaporative cooling at the stratocumulus top, *J. Atmos. Sci.*, doi:10.1175/JAS-D-15-0087.1, in press.
de Roode, S. R., and P. G. Duynkerke (1997), Observed Lagrangian transition of stratocumulus into cumulus during ASTEX: Mean state and turbulence structure, *J. Atmos. Sci.*, *54*(17), 2157–2173.
Deardorff, J. W. (1980), Cloud top entrainment instability, *J. Atmos. Sci.*, *37*(1), 131–147.
Gerber, H., G. Frick, S. P. Malinowski, J.-L. Brenguier, and F. Burnet (2005), Holes and entrainment in stratocumulus, *J. Atmos. Sci.*, *62*, 443–459.
Klingebiel, M., et al. (2015), *Atmos. Chem. Phys.*, *15*(2), 617–631, doi:10.5194/acp-15-617-2015.
Kuo, H.-C., and W. H. Schubert (1988), Stability of cloud-topped boundary layers, *Q. J. R. Meteorol. Soc.*, *114*, 887–916.
Kurowski, M. J., S. P. Malinowski, and W. W. Grabowski (2009), A numerical investigation of entrainment and transport within a stratocumulus-topped boundary layer, *Q. J. R. Meteorol. Soc.*, *135*, 77–92, doi:10.1002/qj.354.
Larson, V. E., K. E. Kotenberg, and N. B. Wood (2007), An analytic longwave radiation formula for liquid layer clouds, *Mon. Weather Rev.*, *135*, 689–699, doi:10.1175/MWR3315.1.
Lilly, D. K. (1968), Models of cloud-topped mixed layers under a strong inversion., *Q. J. R. Metorol. Soc.*, *94*, 292–309.
Lilly, D. K. (2002), Entrainment into mixed layers. Part II: A new closure, *J. Atmos. Sci.*, *59*, 3353–3361.
Lock, A. (1998), The parametrization of entrainment in cloudy boundary layers, *Q. J. R. Metorol. Soc.*, *124*, 2729–2753.
Lock, A., and M. K. MacVean (1999), The parametrization of entrainment driven by surface heating and cloud-top cooling, *Q. J. R. Metorol. Soc.*, *125*, 271–299.
MacVean, M. K., and P. J. Mason (1990), Cloud-top entrainment instability through small-scale mixing and its parameterization in numerical models, *J. Atmos. Sci.*, *47*(8), 1012–1030.
Mellado, J. P. (2010), The evaporatively driven cloud–top mixing layer, *J. Fluid Mech.*, *660*, 5–36, doi:10.1017/S0022112010002831.
Moeng, C. (2000), Entrainment rate, cloud fraction, and liquid water path of PBL stratocumulus clouds, *J. Atmos. Sci.*, *57*(21), 3627–3643, doi:10.1175/1520-0469(2000)057.
Randall, D. A. (1980), Conditional instability of the first kind upside-down, *J. Atmos. Sci.*, *37*(10), 125–130.
Siems, S. T., C. S. Bretherton, M. B. Baker, S. Shy, and R. E. Breidenthal (1990), Buoyancy reversal and cloud-top entrainment instability, *Q. J. R. Meteorol. Soc.*, *116*, 705–739.
Stevens, B. (2002), Entrainment in stratocumulus-topped mixed layers, *Q. J. R. Meteorol. Soc.*, *128*, 2663–2690.
Stevens, B., et al. (2005), Evaluation of large-eddy simulations via observations of nocturnal marine stratocumulus, *Mon. Weather Rev.*, *133*, 1443–1462, doi:10.1175/MWR2930.1.
Turton, J., and S. Nicholls (1987), A study of the diurnal variation of stratocumulus using a multiple mixed layer model, *Q. J. R. Meteorol. Soc.*, *113*(477), 969–1009, doi:10.1256/smsqj.47710.
Wood, R. (2012), Stratocumulus clouds, *Mon. Wea. Rev.*, *140*, 2373–2423.
Yamaguchi, T., and D. A. Randall (2012), Cooling of entrained parcels in a large-eddy simulation, *J. Atmos. Sci.*, *69*, 1118–1136.